Reflection Phase Characterizations of the EBG Ground Plane for Low Profile Wire Antenna Applications

Fan Yang, *Member, IEEE,* and Yahya Rahmat-Samii, *Fellow, IEEE*

***Abstract*—Mushroom-like electromagnetic band-gap (EBG) structures exhibit unique electromagnetic properties that have led to a wide range of electromagnetic device applications. This paper focuses on the reflection phase feature of EBG surfaces: when plane waves normally illuminate an EBG structure, the phase of the reflected field changes continuously from 180° to -180° versus frequency. One important application of this feature is that one can replace a conventional perfect electric conductor (PEC) ground plane with an EBG ground plane for a low profile wire antenna design. For this design, the operational frequency band of an EBG structure is defined as the frequency region within which a low profile wire antenna radiates efficiently, namely, having a good return loss and radiation patterns. The operational frequency band is the overlap of the input-match frequency band and the surface-wave frequency bandgap. It is revealed that the reflection phase curve can be used to identify the input-match frequency band inside of which a low profile wire antenna exhibits a good return loss. The surface-wave frequency bandgap of the EBG surface that helps improve radiation patterns is very close to its input-match frequency band, resulting in an effective operational frequency band. In contrast, a thin grounded slab cannot work efficiently as a ground plane for low profile wire antennas because its surface-wave frequency bandgap and input-match frequency band do not overlap. Parametric studies have been performed to obtain design guidelines for EBG ground planes. Two novel EBG ground planes with interesting electromagnetic features are also presented. The rectangular patch EBG ground plane has a polarization dependent reflection phase and the slotted patch EBG ground plane shows a compact size.**

***Index Terms*—Electromagnetic band-gap (EBG) structures, low profile, reflection phase, wire antenna.**

I. Introduction

In recent years, there has been increasing interest in artificial electromagnetic materials, such as photonic crystals [1], electromagnetic band-gap (EBG) structures [2], [3], and double negative (DNG) materials [4]–[8]. These structures are broadly classified as metamaterials, and are typically realized by periodic dielectric substrates and various metallization patterns [9]–[11]. Metamaterials exhibit novel electromagnetic features which may not occur in nature, and they have led to a wide range of applications in the antenna and propagation fields. For example, EBG structures have been integrated with patch antennas for enhanced performance due to the bandgap of surface-wave suppression [12]–[15]. They have also been used as ground planes of spiral and curl antennas to achieve low profile designs [16], [17].

Of all the interesting properties of metamaterials, the reflection phase feature is of special interest. The reflection phase is defined as the phase of the reflected electric field at the reflecting surface. It is normalized to the phase of the incident electric field at the reflecting surface. It is known that the perfect electric conductor (PEC) has a 180° reflection phase for a normally incident plane wave, while the perfect magnetic conductor (PMC), which does not exist in nature, has a reflection phase of 0°. Much effort has been devoted to realize a PMC-like surface, and some progress has been achieved using hard and soft surfaces [18], [19]. Recent studies on EBG structures have revealed that they can satisfy the PMC-like condition in a certain frequency band [9], [10].

However, EBG structures are more than a PMC surface, as emphasized in this paper. The reflection phase of an EBG surface varies continuously from 180° to −180° versus frequency, not only 180° for a PEC surface or 0° for a PMC surface. This reflection phase feature makes EBG surfaces unique. One potentially important application of this surface is its usage as the ground plane of a wire antenna for a low profile design, which is desirable in many wireless communication systems.

A question arises: what is the suitable frequency band of an EBG ground plane for low profile wire antenna applications? This question is addressed by investigating a mushroom-like EBG surface, as shown in Fig. 1. The mushroom-like structure is known to have an effective bandgap for surface-wave propagation, which can be useful to improve antenna radiation patterns. However, the surface wave band gap cannot guarantee the effective radiation of a low profile wire antenna. This is because complicated interactions occur between the wire antenna and the EBG surface, and electromagnetic waves are not restricted to surface waves that propagate in the horizontal plane. In light of this, a dipole antenna is horizontally positioned near the EBG surface, and its radiation performance is accurately characterized using the FDTD method. By observing both the return losses and radiation patterns of dipoles operating at different frequencies, one can find the useful operational frequency band of the EBG surface. Since the surface-wave frequency bandgap that improves radiation patterns has been thoroughly addressed in [10] and [15], this paper focuses more on the frequency band inside of which an antenna obtains a good return loss. This is defined as the input-match frequency band. Obviously, the op-

Manuscript received September 30, 2002; revised April 23, 2003.

The authors are with the Department of Electrical Engineering, University of California at Los Angeles, Los Angeles, CA 90095-1594 USA (e-mail: ygfn@ee.ucla.edu; rahmat@ee.ucla.edu).

Digital Object Identifier 10.1109/TAP.2003.817559

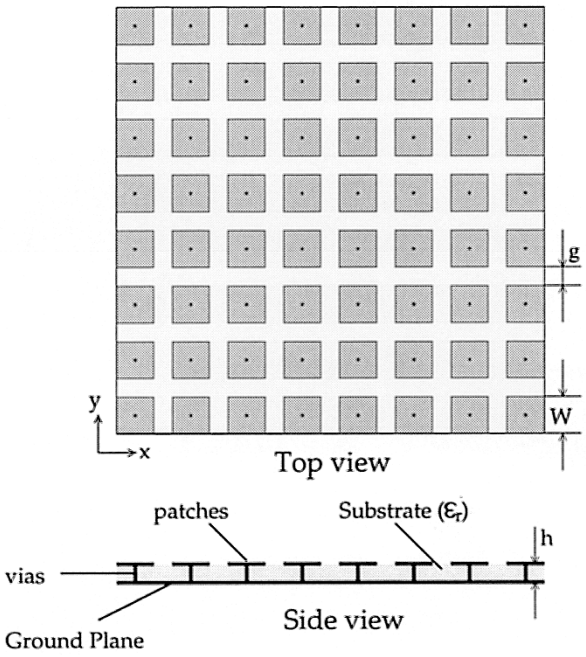

Fig. 1. Geometry of a mushroom-like EBG structure.

erational frequency band is the overlap of the surface-wave frequency bandgap and the input-match frequency band.

Yet another question arises: can the reflection phase feature be used to identify the input-match frequency band? The reason for this question is that it is computationally more efficient to calculate the reflection phase of an EBG surface than to evaluate the radiation performance of several dipole antennas near the EBG surface. In this paper, the procedure to compute the reflection phase using the FDTD method is detailed. It is revealed that the frequency region where the EBG surface has a reflection phase in the range $90^\circ \pm 45^\circ$ is very close to the input-match frequency band. This is ***not*** the frequency region where the EBG surface behaves like the PMC or PEC surface. The quadratic reflection phase allows a low profile wire antenna to obtain a good return loss. Thus, one can use the reflection phase curve to identify the input-match frequency band of the EBG surface.

It is observed that the surface-wave frequency bandgap and the input-match frequency band are close to each other for a mushroom-like EBG surface so that an effective operational frequency band can be obtained. However, it is not necessary that these two frequency bands are similar to each other for a general surface. To further appreciate this point, the performance of a low profile wire antenna on a thin grounded slab is evaluated. In this case a high dielectric constant substrate has to be used to achieve a quadratic reflection phase. Although the wire antenna shows a good return loss, the radiation patterns exhibit bifurcation in the broadside direction and the directivity is decreased due to strong surface waves. Thus, the input-match frequency band does not overlap the surface-wave frequency bandgap in the thin grounded slab case. As a result, there is no effective operational frequency band so that the thin grounded slab cannot work efficiently as the ground plane for low profile wire antennas.

Moreover, some design guidelines for EBG surfaces are obtained by performing parametric studies. The EBG patch width, gap width, substrate permittivity, and substrate thickness are each evaluated. In addition, two novel EBG surfaces are presented: one with a rectangular patch unit and the other with a slotted patch element. The former shows a polarization dependent reflection phase, while the latter has a compact size. Both structures exhibit a good potential for future EBG applications.

II. Frequency Band Selection for Low Profile Wire Antenna Designs

A. Comparison of the PEC, PMC, and EBG Ground Planes

In wireless communications, it is desirable for antennas to be low profile. The low profile design usually refers to the antenna structures whose overall height is less than one tenth of the wavelength at the operating frequency. To this end, a dipole antenna is horizontally positioned near a ground plane. The PEC, PMC, and EBG surfaces are each used as the ground plane to compare their capabilities for low profile antenna designs.

Fig. 2(a) shows a dipole antenna over a PEC or PMC ground plane, and Fig. 2(b) shows a dipole antenna over the EBG ground plane. The dipole length is 0.40 $\lambda_{12\ \mathrm{GHz}}$ and its radius is 0.005 $\lambda_{12\ \mathrm{GHz}}$, while $\lambda_{12\ \mathrm{GHz}}$, the free space wavelength at 12 GHz, is used as a reference length to define the physical dimensions of various EBG and antenna structures studied in this paper. A finite ground plane with 1 $\lambda_{12\ \mathrm{GHz}} \times 1\ \lambda_{12\ \mathrm{GHz}}$ size is used in the analysis. The EBG structure has the following parameters:

$$W = 0.12\ \lambda_{12\ \mathrm{GHz}},\ g = 0.02\ \lambda_{12\mathrm{GHz}},\ h = 0.04\ \lambda_{12\ \mathrm{GHz}},$$
$$r = 0.005\ \lambda_{12\ \mathrm{GHz}},\ \epsilon_r = 2.20 \quad (1)$$

where W is the patch width, g is the gap width, h is the substrate thickness, r is the radius of the vias, and ϵ_r is the substrate permittivity. These dimensions have been chosen as starting design parameters. The height of the dipole over the top surface of the EBG ground plane is 0.02 $\lambda_{12\ \mathrm{GHz}}$. Thus, the overall height of the dipole antenna from the bottom ground plane of the EBG structure is 0.06 $\lambda_{12\ \mathrm{GHz}}$. The dipole height on the PEC and PMC ground plane is then set to 0.06 $\lambda_{12\ \mathrm{GHz}}$ so that all three cases have the same overall height.

Fig. 3 compares the FDTD simulated return loss of a dipole antenna over a PEC, PMC, and EBG ground plane. The input impedance is matched to a 50 Ω transmission line. With the PEC surface as the ground plane, the return loss of the dipole is only -3.5 dB. This is because the PEC surface has a 180° reflection phase, so that the direction of the image current is opposite to that of the original dipole. The reverse image current impedes the efficiency of the radiation of the dipole, resulting in a very poor return loss.

When the PMC surface, which has a reflection phase of 0°, is used as the ground plane the dipole has a return loss of -7.2 dB. This is because a strong mutual coupling occurs between the image current and the dipole due to their close proximity, and the input impedance of the dipole is changed. Therefore, the antenna cannot directly match well to a 50 Ω transmission line. It is realized that one can use a proper impedance transformer

(a) (b)

Fig. 2. Dipole antenna over (a) the PEC or PMC ground plane or (b) the EBG ground plane.

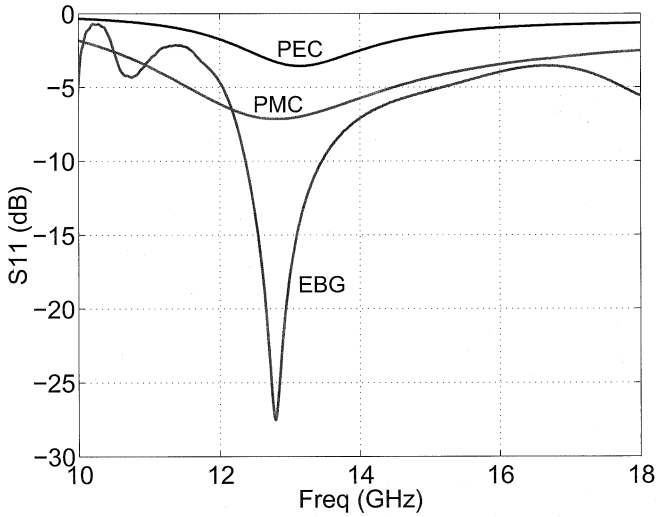

Fig. 3. FDTD simulated return loss results of the dipole antenna over the PEC, PMC, and EBG ground planes. The dipole length is 0.40 $\lambda_{12\ \mathrm{GHz}}$ and the overall antenna height is 0.06 $\lambda_{12\ \mathrm{GHz}}$.

to obtain a good return loss of the dipole. Moreover, the PMC surface is an ideal surface that does not exist in nature.

The best return loss of -27 dB is achieved by the dipole antenna over the EBG ground plane. The reflection phase of the EBG surface varies with frequency from 180° to $-180°$. In a certain frequency band, the EBG surface successfully serves as the ground plane of a low profile dipole, so that the dipole antenna can radiate efficiently. From this comparison it can be seen that the EBG surface is a good ground plane candidate for a low profile wire antenna design.

B. Frequency Band Selection and FDTD Simulation Models

For a mushroom-like surface, a frequency bandgap is defined in [10] using the dispersion diagram. However, this definition only refers to surface waves that propagate in the horizontal plane. In low profile wire antenna applications, such bandgap definition is not applicable because complicated interactions occur between the antenna and the EBG surface, and electromagnetic waves are not restricted to propagate in the horizontal plane.

Therefore, to ensure that resulting EBG designs will meet the criteria of low profile antenna applications, an operational frequency band of an EBG surface is defined as the frequency region inside of which a low profile wire antenna radiates efficiently with a good return loss and radiation patterns. In order to find this operational frequency band, a horizontal dipole antenna is positioned very close to the EBG surface, as shown in Fig. 4(a). The parameters of the EBG surface are fixed and the length of the dipole is changed. If the dipole length is changed, it will resonate at different frequencies. Because the reflection phase of the EBG surface changes with frequency, the return loss of the dipole will change also. The dipole can achieve a good return loss only when the EBG surface has a suitable reflection phase. In addition, the radiation patterns of the dipole are calculated to evaluate the radiation efficiency. Therefore, by observing the return loss and radiation patterns of the dipole at different frequencies, one can find the useful operational frequency band of the mushroom-like surface for low profile wire antenna designs.

It should be emphasized that above operational frequency band of the mushroom-like surface is the overlap of the surface-wave frequency bandgap and the input-match frequency band. Since the surface-wave frequency bandgap that improves radiation patterns has been investigated previously in [10] and [15], this paper focuses more on the input-match frequency band of the mushroom-like surface.

From the computational efficiency viewpoint, it is interesting to know if one could directly use the reflection phase feature of the EBG structure to identify the input-match frequency band. To this end, a plane wave model is established in the FDTD method to evaluate the reflection phase of the EBG surface, as shown in Fig. 4(b). The total field/scattered field formulation is used to incorporate the plane wave excitation into the FDTD method [20]. The plane wave is launched to normally illuminate the EBG structure. The FDTD domain is divided into the total field region and the scattered field region separated by a virtual connecting surface 0.40 $\lambda_{12\ \mathrm{GHz}}$ above the EBG bottom surface. A single unit of the EBG structure with periodic boundary conditions (PBC) on four sides is simulated to model an infinite periodic structure. The perfectly matched layers (PML) are positioned 0.55 $\lambda_{12\ \mathrm{GHz}}$ above the EBG bottom surface.

Since the EBG structure is embedded in the total field region, the reflection phase cannot be directly computed from the reflected field at the EBG top surface. To determine the reflection phase, an observational plane is set at 0.50 $\lambda_{12\ \mathrm{GHz}}$ above the EBG bottom surface so that it is in the scattered field region, and the scattered fields at this plane are recorded. The scattered fields are integrated over the observational plane to determine the reflected field in the far field region in the normal direction. As a reference, the scattered field from a PEC surface are also calculated. The PEC surface is located at the same height of the EBG top surface while the observational plane stays the same. In the same manner, the reflected field from the PEC surface is computed. Then, the reflected field from the EBG structure is divided by the reflected field from the PEC surface. A factor of

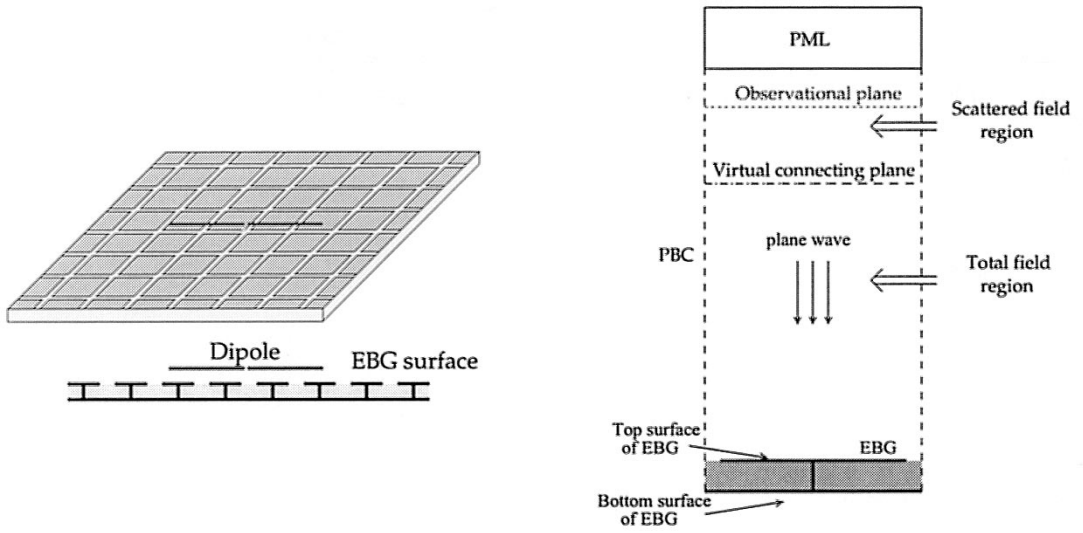

(a) (b)

Fig. 4. FDTD models for input-match frequency band selection of a mushroom-like EBG surface. (a) Low profile dipole antenna over a finite EBG ground plane. (b) Plane wave normally incident upon the EBG surface. In model (b), periodic boundary conditions (PBC) are put around the EBG cell to model an infinite EBG surface and perfect matched layers (PML) are positioned 0.55 $\lambda_{12\ \mathrm{GHz}}$ above the bottom surface of the EBG structure. A virtual surface is put 0.40 $\lambda_{12\ \mathrm{GHz}}$ above the EBG bottom surface to connect the total field region and the scattered field region. The reflected fields at an observational plane 0.50 $\lambda_{12\ \mathrm{GHz}}$ above the EBG bottom surface are recorded.

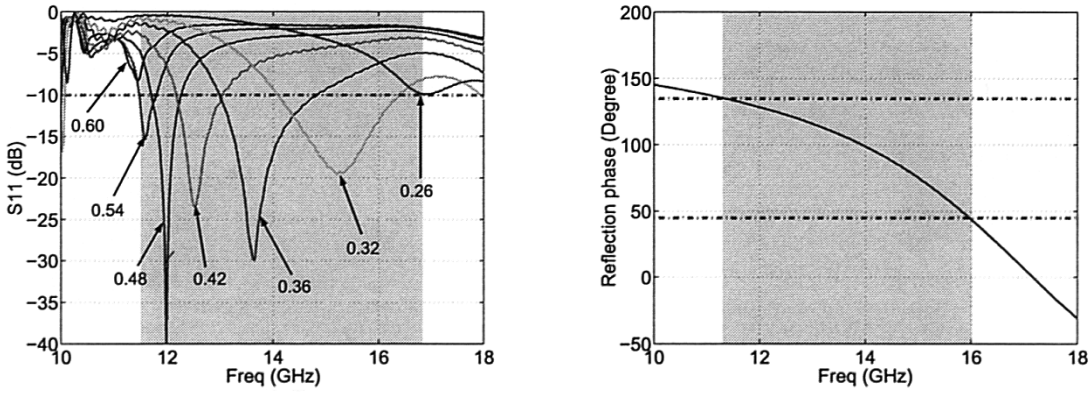

(a) (b)

Fig. 5. Comparison of two FDTD model results of the EBG surface described in (1). (a) Return loss of the dipole with its length varying from 0.26 $\lambda_{12\ \mathrm{GHz}}$ to 0.60 $\lambda_{12\ \mathrm{GHz}}$. (b) Reflection phase of the EBG surface. The frequency band of the dipole model is 11.5–16.6 GHz according to -10 dB return loss criterion. The frequency band of the plane wave model is 11.3–16 GHz for $90^\circ \pm 45^\circ$ reflection phase region.

π is added to the phase to account for the reference of the PEC surface, which is known to have a reflection phase of π radians. The EBG reflection phase characterization obtained from the above procedure follows the same methodology applied in [10], [21], [22]. This model only depends on the EBG surface itself.

The simulation results of the low profile dipole model and plane wave illumination model are compared to each other in order to establish a methodology as how to use the reflection phase curve to identify the input-match frequency band.

C. Frequency Band Results

The EBG surface analyzed here has the same parameters as (1). Fig. 5(a) shows the return loss results of a dipole with its length varying from 0.26 $\lambda_{12\ \mathrm{GHz}}$ to 0.60 $\lambda_{12\ \mathrm{GHz}}$. The radius of the dipole remains 0.005 $\lambda_{12\ \mathrm{GHz}}$. In order to locate the dipole very close to the EBG ground plane, the height of the dipole is set to 0.02 $\lambda_{12\ \mathrm{GHz}}$, which is only one cell above the EBG ground plane in the FDTD simulation. A finite EBG ground plane of 1 $\lambda_{12\ \mathrm{GHz}} \times 1\ \lambda_{12\ \mathrm{GHz}}$ is used in the analysis, and the dipole is positioned in the center of the ground plane for symmetrical patterns. The dipole shows a return loss better than -10 dB from 11.5 to 16.6 GHz. Thus, the input-match frequency band is from 11.5 to 16.6 GHz.

Fig. 5(b) shows the reflection phase results of the plane wave model. In contrast to the 180° reflection phase of the PEC surface and 0° reflection phase of the PMC surface, if one chooses the $90^\circ \pm 45^\circ$ reflection phases as criterion for the EBG surface, a frequency region from 11.3 to 16 GHz can be obtained, which is nearly the same frequency region as the input-match frequency band.

From these calculations, it is revealed that the reflection phase feature of an EBG surface can be used to identify the input-

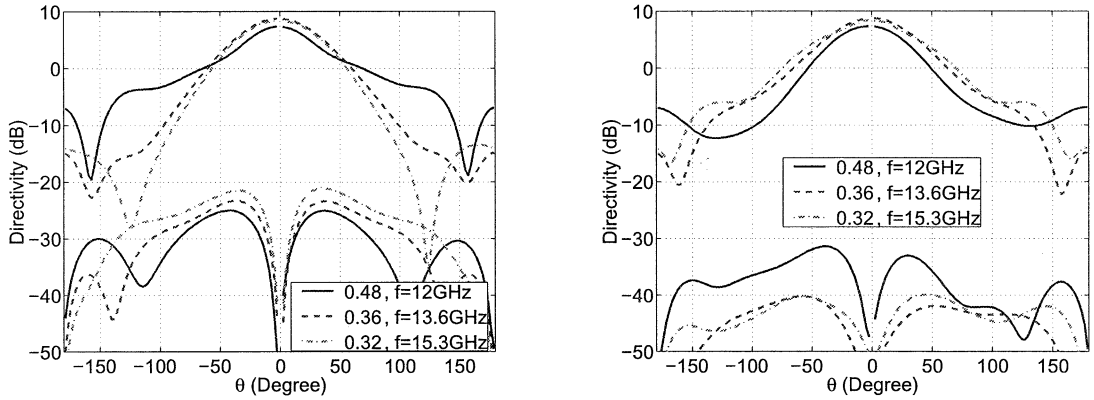

Fig. 6. Radiation patterns of three dipoles at their resonant frequencies. (a) E-plane pattern. (b) H-plane pattern. The 0.48 $\lambda_{12\ \mathrm{GHz}}$ dipole resonates at 12 GHz, the 0.36 $\lambda_{12\ \mathrm{GHz}}$ dipole resonates at 13.6 GHz, and the 0.32 $\lambda_{12\ \mathrm{GHz}}$ dipole resonates at 15.3 GHz. The radiation patterns show that dipoles radiate efficiently throughout the frequency band in Fig. 5.

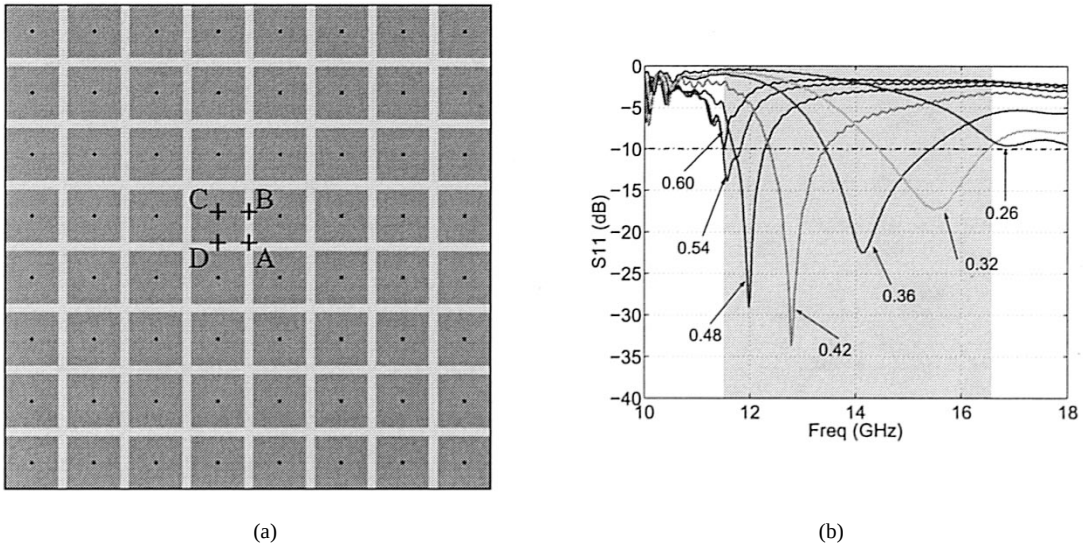

Fig. 7. Positional effect of the dipole on the input-match frequency band selection of the EBG surface. (a) Various dipole positions ("+" represents the center of the dipole). (b) Return loss of the dipole located at position C with its length varying from 0.26 $\lambda_{12\ \mathrm{GHz}}$ to 0.60 $\lambda_{12\ \mathrm{GHz}}$. The dipole can match well from 11.5–16.5 GHz that is very close to the result in Fig. 5(a) when the dipole is located at position A. Similar observations were made at the position B and D.

match frequency band for low profile wire antenna applications. The input-match frequency band is the frequency region where the EBG surface shows a reflection phase in the range $90° \pm 45°$. The quadratic phase is necessary for a low profile wire antenna to obtain a good return loss.

The radiation patterns of dipole antennas on the EBG surface are also calculated using the FDTD method. Fig. 6 displays both the E- and H-plane patterns of three dipole antennas at their resonant frequencies: 1) a 0.48 $\lambda_{12\ \mathrm{GHz}}$ dipole, which resonates at 12 GHz; 2) a 0.36 $\lambda_{12\ \mathrm{GHz}}$ dipole, which resonates at 13.6 GHz; and 3) a 0.32 $\lambda_{12\ \mathrm{GHz}}$ dipole, which resonates at 15.3 GHz. It is observed that all dipoles have directivities around 8 dB. The good radiation patterns benefit from the surface-wave frequency bandgap. As revealed in [15], the mushroom-like surface exhibits a surface-wave frequency bandgap that has a similar position as the input-match frequency band identified in Fig. 5(a). Therefore, the operational frequency band of the mushroom-like surface, as the overlap of these two frequency bands, also has the similar frequency region. It is important to point out that the input-match frequency band and the surface-wave frequency bandgap are not necessarily to be close to each other for a general surface, which will be clarified in the Section II.D.

The return loss results shown in Fig. 5(a) are for dipoles whose centers are located between EBG patches at position A, as shown in Fig. 7(a). Dipoles with different center locations have been simulated to test the positional effect of the dipole model. Fig. 7(b) shows the return loss results of dipoles whose centers are located at position C. Although the return loss may change a bit for each dipole, it still exhibits a return loss better than -10 dB inside the input-match frequency band obtained in Fig. 5. Simulations of dipoles at positions B and D were performed, and the same input-match frequency band results were observed. In addition, it is worthwhile to point out that the ground plane size effect was also considered. A $2\ \lambda_{12\ \mathrm{GHz}} \times 2\ \lambda_{12\ \mathrm{GHz}}$ EBG ground plane was used in the dipole model, and the simulation results provided the same input-match frequency band.

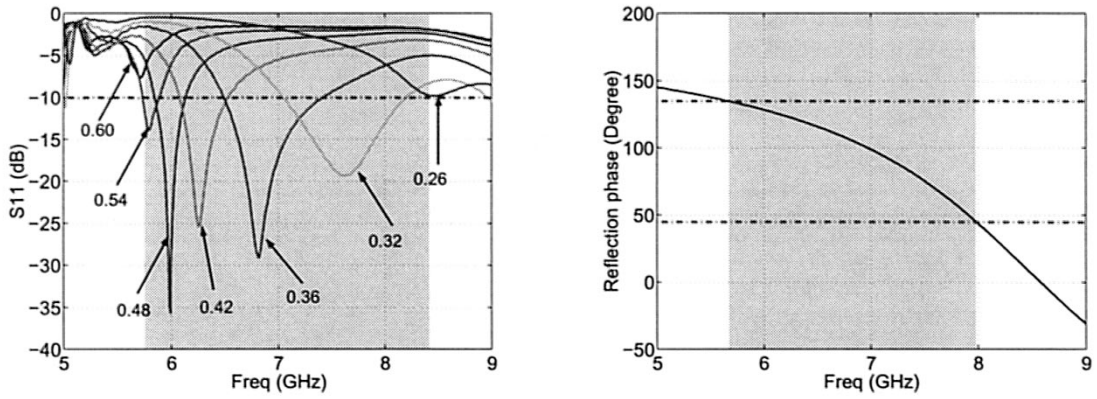

(a) (b)

Fig. 8. Comparison of two FDTD model results of the EBG surface described in (2). (a) Return loss of the dipole with its length varying from 0.26 $\lambda_{6\ \mathrm{GHz}}$ to 0.60 $\lambda_{6\ \mathrm{GHz}}$. (b) Reflection phase of the EBG surface. The frequency band of the dipole model is 5.8–8.3 GHz according to -10 dB return loss criterion. The frequency band of the plane wave model is 5.7–8.0 GHz for $90^\circ \pm 45^\circ$ reflection phase region.

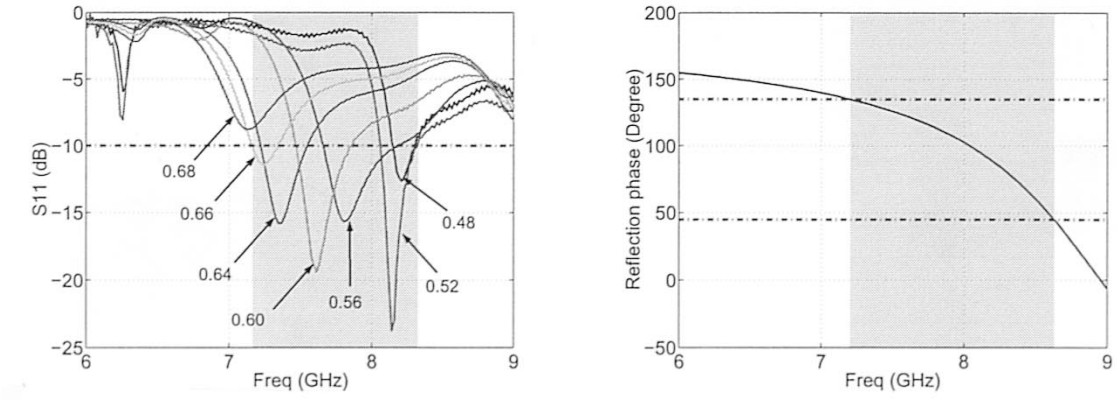

(a) (b)

Fig. 9. Comparison of two FDTD model results of the EBG surface with a high permittivity substrate: (a) return loss of the dipole with its length varying from 0.48 $\lambda_{12\ \mathrm{GHz}}$ to 0.68 $\lambda_{12\ \mathrm{GHz}}$ and (b) reflection phase of the EBG surface. The frequency band of the dipole model is 7.2–8.3 GHz according to -10 dB return loss criterion. The frequency band of the plane wave model is 7.2–8.6 GHz for $90^\circ \pm 45^\circ$ reflection phase region.

To further verify the observation on the input-match frequency band selection, two more cases are investigated. The first EBG case has the same dielectric constant as (1), but now the other parameters such as patch width, height, and gap width are doubled. They are listed below

$$W = 0.12\ \lambda_{6\ \mathrm{GHz}},\ g = 0.02\ \lambda_{6\ \mathrm{GHz}},\ h = 0.04\ \lambda_{6\ \mathrm{GHz}},$$
$$r = 0.005\ \lambda_{6\ \mathrm{GHz}},\ \epsilon_r = 2.20. \tag{2}$$

$\lambda_{6\ \mathrm{GHz}}$ is the free space wavelength at 6 GHz. Fig. 8 shows the reflection phase results of the EBG surface and the return loss results of dipoles with varying lengths from 0.26 $\lambda_{6\ \mathrm{GHz}}$ to 0.60 $\lambda_{6\ \mathrm{GHz}}$, and a fixed height of 0.02 $\lambda_{6\ \mathrm{GHz}}$. The dipole shows a good return loss from 5.8 to 8.3 GHz, which is close to the frequency region (5.7–8.0 GHz, 33.5%) where the reflection phase of the EBG surface is in the range $90^\circ \pm 45^\circ$. The radiation patterns are calculated and the results are similar to Fig. 6. This simulation also demonstrates that the EBG structure is scalable.

The second EBG case has the same parameters as (1), except that the dielectric constant is increased to 10.2. The dipole length varies from 0.48 $\lambda_{12\ \mathrm{GHz}}$ to 0.68 $\lambda_{12\ \mathrm{GHz}}$, and the results are shown in Fig. 9. The frequency region of the reflection phase in the range $90^\circ \pm 45^\circ$ is from 7.2 to 8.6 GHz (17.7%), inside which low profile dipoles exhibit good return loss results. It is noticed that the bandwidth becomes narrower because the dielectric constant is increased.

Moreover, the input-match frequency band selection criteria has been verified by experimental results of a low profile curl antenna over the EBG ground plane. A detailed description of the curl antenna and the EBG ground plane design is published by the authors in [17]. The EBG structure has the same parameters as (2), and the frequency region where the EBG surface exhibits a reflection phase around 90° is used to achieve a good return loss of the curl antenna. The satisfactory performance of this antenna design demonstrates the usefulness of the selection criteria discussed earlier.

D. Thin Grounded High Dielectric Constant Slab

It is instructive to compare the EBG surface with a thin grounded high dielectric constant slab. The reflection coefficient R of the grounded slab for a normally incident plane wave can be calculated from the following equation:

$$R = \frac{\sqrt{\epsilon_r}\cos(k_1 h) - j\sin(k_1 h)}{\sqrt{\epsilon_r}\cos(k_1 h) + j\sin(k_1 h)} \tag{3}$$

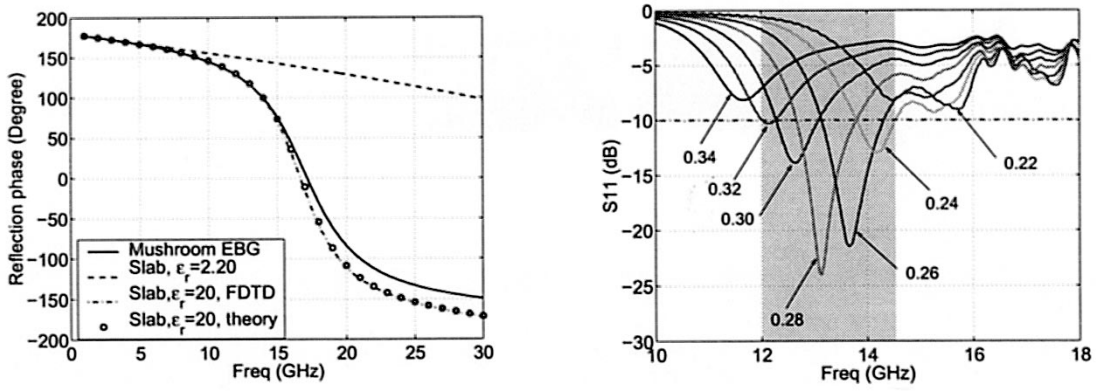

(a) (b)

Fig. 10. Thin grounded high dielectric constant slab. (a) Reflection phase results. (b) Return loss results of the dipole near the slab with its length varying from 0.22 $\lambda_{12\ \mathrm{GHz}}$ to 0.34 $\lambda_{12\ \mathrm{GHz}}$. The dielectric constant of the substrate has to be increased to 20 in order to get a similar reflection phase as the EBG surface. The dipole can obtain a good return loss in the frequency region where the slab has a reflection phase around 90°.

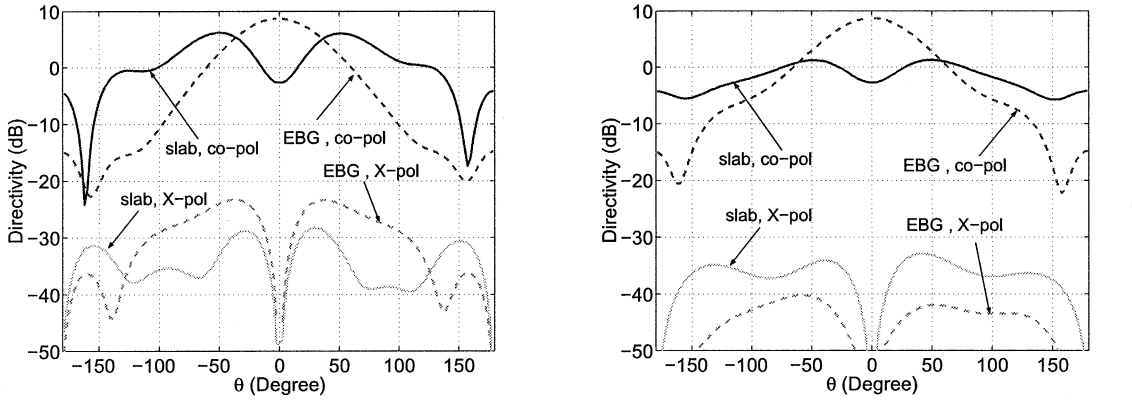

(a) (b)

Fig. 11. Radiation pattern comparison of dipoles near the thin grounded high dielectric constant slab and the EBG surface. (a) E-plane pattern. (b) H-plane pattern. The patterns are calculated at the resonant frequency of 13.6 GHz. Since the high dielectric constant substrate is used in the grounded slab and strong surface waves are excited, the dipole on the slab shows a lower gain and higher back lobe.

where ϵ_r is the dielectric constant of the substrate, h is the thickness of the substrate, and k_1 is the wave number in the substrate. Fig. 10(a) shows the reflection phase results of grounded slabs compared to the EBG surface analyzed in Fig. 5. The thickness of the slab is 0.04 $\lambda_{12\ \mathrm{GHz}}$, which is the same as the EBG surface. When the slab has the same dielectric constant of 2.20 as the EBG surface, it shows a larger reflection phase than the EBG surface. In order to obtain a similar reflection phase as the EBG surface, the dielectric constant must be increased to 20. It is also observed that the FDTD results agree very well with the analytic results, which proves the accuracy of the FDTD codes developed at the UCLA antenna lab.

The return loss results of dipoles on the grounded slab are plotted in Fig. 10(b). The height of the dipole is 0.02 $\lambda_{12\ \mathrm{GHz}}$, the same as the EBG case, and its length varies from 0.22 $\lambda_{12\ \mathrm{GHz}}$ to 0.34 $\lambda_{12\ \mathrm{GHz}}$. It is noticed that although the length becomes shorter, it can still obtain a good return loss in the frequency region where the reflection phase of the slab is around 90°. This result further demonstrates the usefulness of the quadratic reflection phase.

However, the return loss is only one aspect of the antenna performance: the radiation pattern should also be considered. In light of this, the radiation patterns of a dipole on the grounded slab are calculated and compared to a dipole on the EBG surface. Fig. 11 shows the E- and H-plane pattern comparisons of two dipoles: one is a 0.26 $\lambda_{12\ \mathrm{GHz}}$ dipole on the grounded slab with $\epsilon_r = 20$, and the other is a 0.36 $\lambda_{12\ \mathrm{GHz}}$ dipole on the EBG surface. Both antennas resonate at 13.6 GHz with return losses better than -20 dB. The ground plane size is 1 $\lambda_{12\ \mathrm{GHz}} \times 1\ \lambda_{12\ \mathrm{GHz}}$ for both cases. The radiation patterns of the dipole on the slab exhibit bifurcation in the broadside direction. This is because the high dielectric constant substrate is used in the slab case, and the 0.04 $\lambda_{12\ \mathrm{GHz}}$ thickness is equal to 0.20 λ_g at 13.6 GHz. λ_g is the guided wavelength in the substrate. Therefore, most of the energy from the dipole is converted to surface waves, and the edge diffractions of the surface waves form the interference patterns. In this case the dipole becomes an effective surface-wave transducer rather than a radiating element. In contrast, since the EBG surface can prevent surface-wave propagation, the dipole on the EBG surface shows a higher gain and lower back lobe.

In summary, the EBG surface whose surface-wave frequency bandgap and input-match frequency band have similar frequency regions is a good ground plane for low profile wire

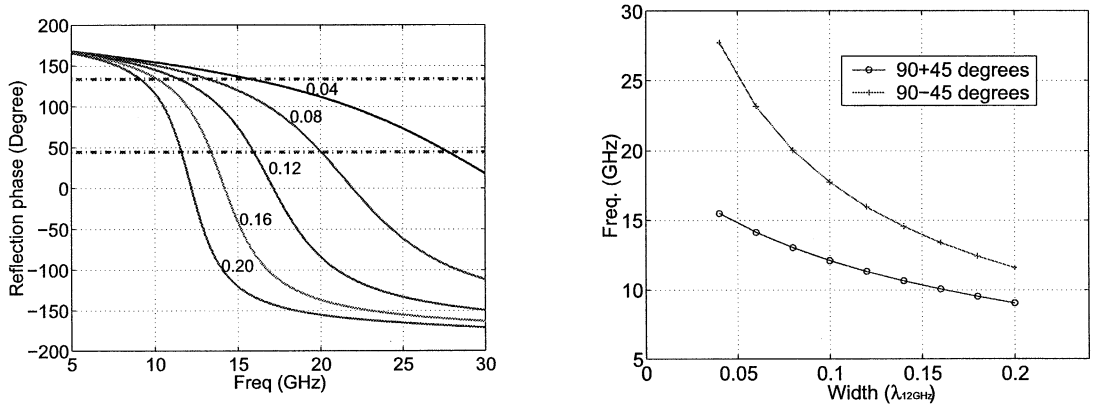

(a) (b)

Fig. 12. EBG parameters analysis: patch width effect. (a) Reflection phases of plane waves. (b) Frequency band of the EBG structure versus patch width. When the patch width W is increased from 0.04 $\lambda_{12\ \mathrm{GHz}}$ to 0.20 $\lambda_{12\ \mathrm{GHz}}$, the frequency band position and bandwidth decrease.

antennas, whereas the thin grounded slab is not because its surface-wave frequency bandgap at the low frequency region does not overlap its input-match frequency band.

III. Parametric Study of the EBG Surface

It has been revealed that the input-match frequency band of an EBG surface for low profile wire antenna applications is the frequency region where the EBG surface has a reflection phase in the range $90° \pm 45°$. The reflection phase of the mushroom-like EBG surface is mainly determined by four parameters (see Fig. 1): patch width (W), gap width (g), substrate permittivity (ϵ_r), and substrate thickness (h). In this section, the effects of these parameters are discussed one by one in order to obtain some engineering design guidelines for EBG surfaces. Since the FDTD method takes into account complete electrodynamics in the EBG structures, it is more accurate than other lumped element models. In addition, the FDTD method can deal with general topologies such as a complex slot loaded EBG structure described in the next section. The frequency band discussed in this section refers to the input-match frequency band. In conjunction with the surface-wave bandgap, it can provide a useful operational frequency band for low profile wire antenna designs.

A. Patch Width Effect

Patch width plays an important role in determining the frequency band. To study the effect of the EBG patch width, other parameters such as the gap width, substrate permittivity, and substrate thickness are kept the same as in (1). The patch width is changed from 0.04 $\lambda_{12\ \mathrm{GHz}}$ to 0.20 $\lambda_{12\ \mathrm{GHz}}$.

Fig. 12(a) shows the reflection phases of plane waves illuminating the EBG surfaces with different patch widths. In addition, Fig. 12(b) presents the frequency band versus the patch width, and Table I lists the frequency band data at different patch widths. $90° \pm 45°$ reflection phases are used as the criterion to determine the frequency band. It is observed that when the patch width is increased, the frequency band position and its bandwidth decrease. For example, when the patch width is 0.04 $\lambda_{12\ \mathrm{GHz}}$, the frequency band ranges from 15.49 to 27.72 GHz, resulting in a 56.6% bandwidth. When the patch width is increased to 0.20 $\lambda_{12\ \mathrm{GHz}}$, the frequency band decreases and ranges from 9.07 to 11.61 GHz. The bandwidth also becomes narrower, lowering to 24.6%.

TABLE I
Parameter Analysis of the EBG Structure: Patch Width Effect

Patch width (λ_{12GHz})	$f_{\phi=135°}(GHz)$	$f_{\phi=45°}(GHz)$	Band width (GHz)	BW (%)
0.04	15.49	27.72	12.23	56.6%
0.06	14.14	23.16	9.02	48.4%
0.08	13.04	20.03	6.99	42.3%
0.10	12.12	17.74	5.62	37.6%
0.12	11.34	15.97	4.63	33.9%
0.14	10.66	14.56	3.90	30.9%
0.16	10.07	13.40	3.33	28.4%
0.18	9.54	12.43	2.89	26.3%
0.20	9.07	11.61	2.54	24.6%

B. Gap Width Effect

The gap width is the distance between adjacent patches. It controls the coupling of EBG patch units. Variation of the gap width affects the frequency band of the EBG surface. During this investigation, the patch width, substrate permittivity, and substrate thickness are kept the same as in (1). The gap width is increased from 0.01 $\lambda_{12\ \mathrm{GHz}}$ to 0.12 $\lambda_{12\ \mathrm{GHz}}$. When the gap width is increased to 0.12 $\lambda_{12\ \mathrm{GHz}}$, the gap width becomes the same as the patch width.

Fig. 13(a) displays the reflection phases with different gap widths, and Fig. 13(b) presents the frequency band versus the gap width. Table II lists the frequency band data at different gap widths. When the gap width is only 0.01 $\lambda_{12\ \mathrm{GHz}}$, the frequency band of the EBG surface is from 10.08 to 13.45 GHz and the bandwidth is 28.6%. The frequency band increases to cover 14.64–22.85 GHz with a 43.8% bandwidth when the gap width is increased to 0.12 $\lambda_{12\ \mathrm{GHz}}$. Therefore, the variation in the gap width has the opposite effect to the variation in the patch width: as the gap width increases, both the frequency band position and the bandwidth increase.

C. Substrate Permittivity Effect

Relative permittivity (ϵ_r), also called the dielectric constant of a substrate, is another effective parameter used to control the

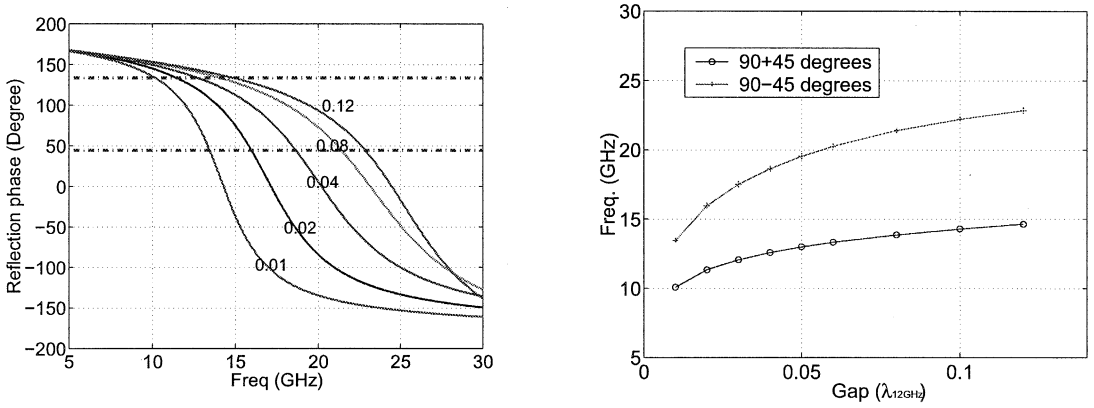

(a) (b)

Fig. 13. EBG parameters analysis: gap width effect. (a) Reflection phases of plane waves. (b) Frequency band of the EBG structure versus gap width. When the gap width g is increased from 0.01 $\lambda_{12\ \mathrm{GHz}}$ to 0.12 $\lambda_{12\ \mathrm{GHz}}$, both the frequency band position and its bandwidth increase.

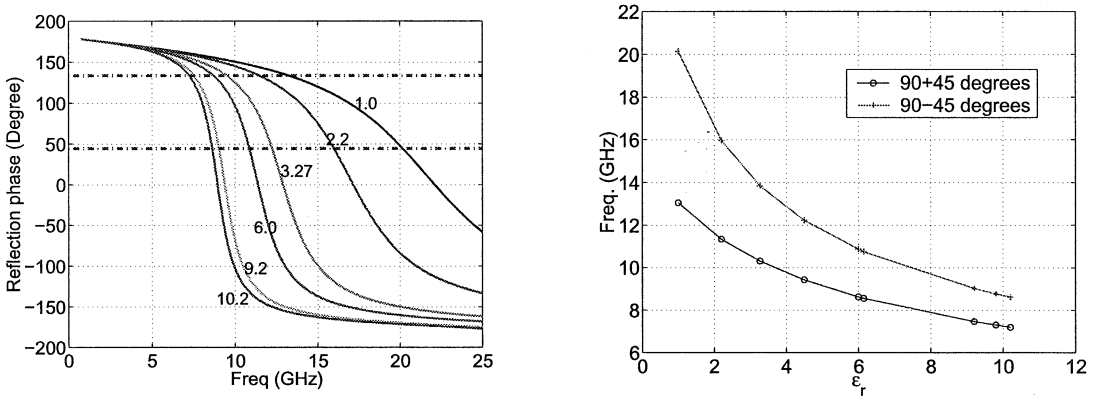

(a) (b)

Fig. 14. EBG parameters analysis: permittivity effect. (a) Reflection phases of plane waves. (b) Frequency band of the EBG structure versus substrate permittivity. When the substrate permittivity ϵ_r is increased, the frequency band position and bandwidth decreases.

TABLE II
PARAMETER ANALYSIS OF THE EBG STRUCTURE: GAP WIDTH EFFECT

Gap width (λ_{12GHz})	$f_{\phi=135^\circ}(GHz)$	$f_{\phi=45^\circ}(GHz)$	Band width (GHz)	BW (%)
0.01	10.08	13.45	3.37	28.6%
0.02	11.34	15.97	4.63	33.9%
0.03	12.07	17.52	5.45	36.8%
0.04	12.58	18.65	6.07	38.9%
0.05	12.99	19.54	6.55	40.3%
0.06	13.32	20.27	6.95	41.4%
0.08	13.86	21.40	7.54	42.8%
0.10	14.29	22.23	7.94	43.5%
0.12	14.64	22.85	8.21	43.8%

TABLE III
PARAMETER ANALYSIS OF THE EBG STRUCTURE: PERMITTIVITY EFFECT

material	ϵ_r	$f_{\phi=135^\circ}(GHz)$	$f_{\phi=45^\circ}(GHz)$	Band width (GHz)	BW (%)
Air	1.0	13.06	20.14	7.08	42.7%
R/D 5880	2.20	11.34	15.97	4.63	33.9%
TMM 3	3.27	10.31	13.85	3.54	29.3%
TMM 4	4.50	9.43	12.23	2.8	25.9%
TMM 6	6.10	8.64	10.87	2.23	22.9%
R/D 6006	6.15	8.57	10.75	2.18	22.6%
TMM 10	9.2	7.47	9.03	1.56	18.9%
TMM 10i	9.8	7.31	8.78	1.47	18.3%
R/D 6010	10.2	7.20	8.63	1.43	18.1%

frequency band. Some commonly used commercial materials such as RT/duroid substrates and TMM substrates are investigated, as well as air. The EBG structure analyzed here has the same parameters as (1), except that the permittivity is changed.

The reflection phases and frequency band positions of various permittivities are plotted in Fig. 14, and some representative data are listed in Table III. It is observed that when air is used as the substrate, the EBG surface has the highest frequency band (13.06–20.14 GHz) and largest bandwidth (42.7%). When the permittivity is increased, the frequency band decreases, as does the bandwidth. Therefore, when the RT/Duroid 6010 substrate ($\epsilon_r = 10.2$) is used, the frequency band lowers to 7.20–8.63 GHz, and the bandwidth decreases to 18.1%.

D. Substrate Thickness and Vias Effect

The substrate thickness is always kept small because a thin EBG surface is desired. In the following simulations the patch width, gap width, and substrate permittivity are the same as in

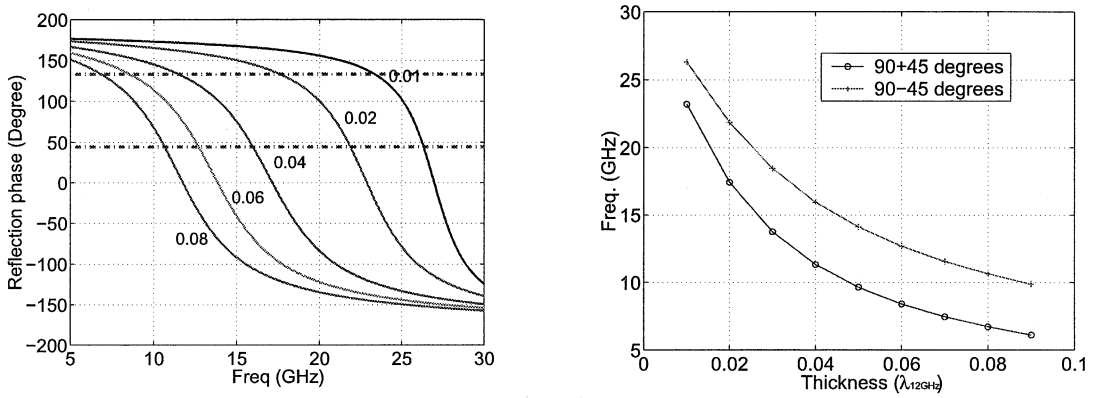

(a) (b)

Fig. 15. EBG parameters analysis: substrate thickness effect. (a) Reflection phases of plane waves. (b) Frequency band of the EBG structure versus substrate thickness. When the substrate thickness h is increased from 0.01 $\lambda_{12\ \mathrm{GHz}}$ to 0.08 $\lambda_{12\ \mathrm{GHz}}$, the frequency band position decreases while its bandwidth increases.

TABLE IV
PARAMETER ANALYSIS OF THE EBG STRUCTURE: SUBSTRATE THICKNESS EFFECT

Thickness (λ_{12GHz})	$f_{\phi=135^\circ}(GHz)$	$f_{\phi=45^\circ}(GHz)$	Band width (GHz)	BW (%)
0.01	23.21	26.30	3.09	12.5%
0.02	17.44	21.86	4.42	22.5%
0.03	13.76	18.46	4.7	29.2%
0.04	11.34	15.97	4.33	33.9%
0.05	9.66	14.12	4.46	37.5%
0.06	8.42	12.69	4.27	40.5%
0.07	7.47	11.57	4.10	43.1%
0.08	6.72	10.64	3.92	45.2%
0.09	6.12	9.88	3.76	47.0%

(1). The substrate thickness is changed from 0.01 $\lambda_{12\ \mathrm{GHz}}$ to 0.09 $\lambda_{12\ \mathrm{GHz}}$.

The reflection phases with different substrate thicknesses are shown in Fig. 15(a), and the frequency band position versus substrate thickness is shown in Fig. 15(b). It is observed that if the substrate thickness is increased, the frequency band will decrease. For instance, the frequency band of the $h = 0.01\ \lambda_{12\ \mathrm{GHz}}$ case is from 23.21 to 26.30 GHz. When the substrate thickness is increased to 0.09 $\lambda_{12\ \mathrm{GHz}}$, the frequency band decreases to 6.12–9.88 GHz. This is similar to the effect of patch width and permittivity. However, in contrast to those parameters, the bandwidth increases with the substrate thickness. As listed in Table IV, the bandwidth is only 12.5% for the $h = 0.01\ \lambda_{12\ \mathrm{GHz}}$ case, while it is 47.0% for the $h = 0.09\ \lambda_{12\ \mathrm{GHz}}$ case.

When the substrate thickness is increased, the length of the vias also increases. According to the LC model [10], the frequency band will decrease. This is consistent with the FDTD simulation results. In addition, the radius effect of the vias was considered. EBG cases with vias' radius varying from 0.001 $\lambda_{12\ \mathrm{GHz}}$ to 0.009 $\lambda_{12\ \mathrm{GHz}}$ were simulated, and it was noticed that the radius has little effect on the frequency band due to the thin vias used.

IV. NOVEL EBG SURFACE DESIGNS

Having obtained design guidelines, one can create novel EBG configurations. For example, previous research focuses on EBG surfaces with square patch units. If the EBG patch unit is modified, different functionalities can be realized. This section analyzes two novel EBG structures. One is a rectangular patch EBG surface whose reflection phase is dependent on the polarization of the incident plane wave. The other is a slotted patch EBG structure that has a compact unit size.

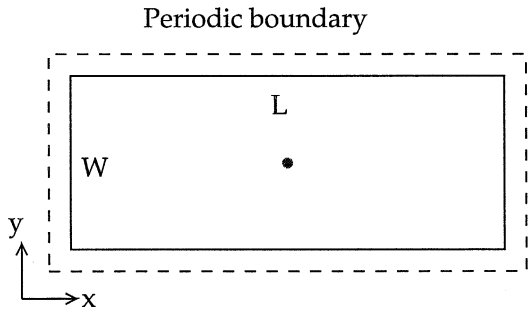

Fig. 16. Polarization dependent EBG surface using rectangular patches with central vias. The length L of the patch is 0.20 $\lambda_{12\ \mathrm{GHz}}$ and the width W is 0.08 $\lambda_{12\ \mathrm{GHz}}$. The gap width is 0.02 $\lambda_{12\ \mathrm{GHz}}$. The substrate thickness is 0.04 $\lambda_{12\ \mathrm{GHz}}$ and its permittivity is 2.20.

A. Rectangular Patch EBG Surface

Since the normal EBG structure uses a square patch as its element, it is symmetric in the x and y direction, as shown in Fig. 16. Thus, the reflection phase is independent of the polarization direction of the normally incident plane wave. When rectangular patches are implemented in the EBG surface, the reflection phase feature changes. Fig. 16 plots a rectangular patch element of the EBG surface. Along the x axis, the patch length is L, and along the y axis, the patch width is W, such that $W < L$. Therefore, the reflection phase of the plane wave is different depending on the x- or y-polarization direction.

The rectangular patch EBG structure has the following parameters:

$$L = 0.20\ \lambda_{12\ \mathrm{GHz}},\ W = 0.08\ \lambda_{12\ \mathrm{GHz}},\ g = 0.02\ \lambda_{12\ \mathrm{GHz}},$$
$$h = 0.04\ \lambda_{12\ \mathrm{GHz}},\ r = 0.005\ \lambda_{12\ \mathrm{GHz}},\ \epsilon_r = 2.20. \quad (4)$$

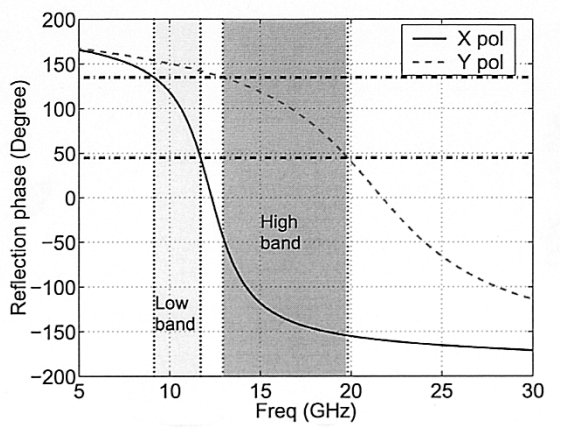

Fig. 17. Reflection phase of the polarization dependent EBG surface. The EBG surface shows two different frequency bands corresponding to the x-polarized and y-polarized plane waves.

Fig. 17 shows the reflection phases of x- and y-polarized plane waves. When the incident plane wave is x-polarized, the patch length (L) has a dominant effect. Since L is large, the frequency band is low according to the previous parametric study on the patch width. The frequency band for an x-polarized wave is 9.14–11.7 GHz. When the incident plane wave is y-polarized, the patch width (W) plays an important role. The frequency frequency band becomes higher due to the smaller width. The frequency band for a y-polarized wave ranges from 12.93 to 19.82 GHz. Therefore, this EBG structure can obtain two different frequency bands corresponding to two different polarized plane waves.

This EBG structure can be implemented to various antenna designs. One potential application is to use this EBG surface to change antenna polarizations. Such a design can be utilized in space and personal communication systems.

B. Slotted Patch EBG Surface

Compactness is always of importance in wireless communications. There are various methods to reduce the EBG size, such as multilayer EBG structures. In this section a novel compact design is suggested, called slotted patch EBG design. It is known that slots on microstrip patch antennas help reduce the antenna size because they change the current distribution on the patch [23]. This idea is also applied in the EBG design.

A slotted patch element is displayed in Fig. 18, with a square patch being used in this design. The parameters of the EBG structure are

$$W = 0.12\,\lambda_{12\ \mathrm{GHz}},\ g = 0.02\,\lambda_{12\ \mathrm{GHz}},\ h = 0.04\,\lambda_{12\ \mathrm{GHz}},$$
$$r = 0.005\,\lambda_{12\ \mathrm{GHz}},\ \epsilon_r = 2.20. \tag{5}$$

Four identical slots are cut on the patch for miniaturization. The slot length is 0.09 $\lambda_{12\ \mathrm{GHz}}$, and its width is 0.01 $\lambda_{12\ \mathrm{GHz}}$. The distance between the slot and patch edge is 0.01 $\lambda_{12\ \mathrm{GHz}}$. These dimensions are selected from many FDTD simulations to achieve the optimum miniaturization effect.

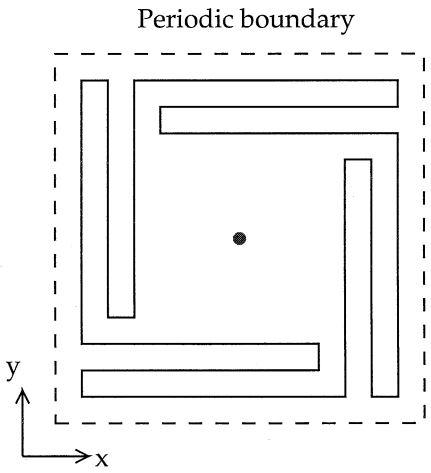

Fig. 18. Compact EBG surface using slotted patches with central vias. Four 0.09 $\lambda_{12\ \mathrm{GHz}}$ long slots are cut onto a square patch. The slot width is 0.01 $\lambda_{12\ \mathrm{GHz}}$, and the distance between slot and patch edge is 0.01 $\lambda_{12\ \mathrm{GHz}}$.

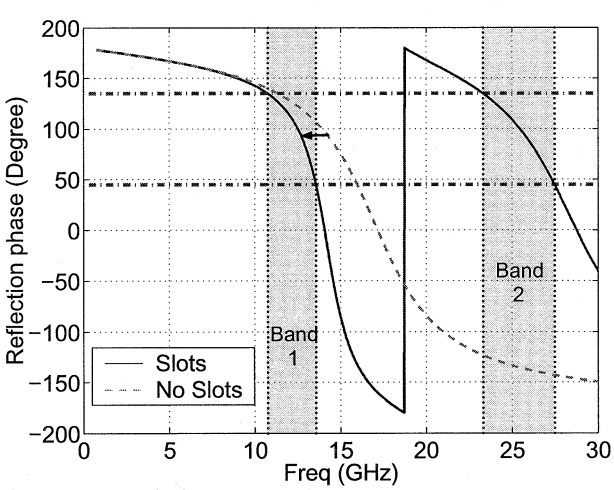

Fig. 19. Reflection phase of the compact slotted patch EBG surface. When the slots are cut onto the patch, the frequency band position decreases. A second frequency band is also observed at around 25 GHz.

The reflection phase of this EBG structure is depicted in Fig. 19, and it is compared to a normal EBG surface without the four slots. In the latter case, the frequency frequency ranges from 11.34–15.97 GHz. When the slots are incorporated, the frequency band decreases to 10.75–13.56 GHz. The similar frequency band position can be obtained using a normal EBG structure without slots, which has the same gap width and substrate properties, but a larger patch size of 0.14 $\lambda_{12\ \mathrm{GHz}}$. Thus, a 14% size reduction is achieved using this slotted patch design. This design can be combined with other approaches for further compact EBG designs.

Another interesting observation of the slotted patch EBG surface is that a second frequency band is noted. When using a normal EBG structure, only one band can be observed below 30 GHz. Once the slots are cut, they reduce the reflection phase frequency. Not only does the basic frequency band decrease, the frequency band of the higher mode is also reduced. Thus, a second band appears around 25 GHz.

V. Conclusion

This paper presents a detailed study on the reflection phase feature of a mushroom-like EBG surface. It is revealed that the EBG ground plane requires a reflection phase in the range of $90^\circ \pm 45^\circ$ for a low profile wire antenna to obtain a good return loss. Thus, one could use the reflection phase curve to identify the input-match frequency band. It is also observed that the surface-wave frequency bandgap of the mushroom-like surface is very close to its input-match frequency band, resulting in an effective operational frequency band. Thus, a low profile wire antenna radiates efficiently near the EBG surface with a good return loss and radiation patterns. In contrast, a thin grounded slab whose surface-wave frequency bandgap and input-match frequency band do not overlap cannot work efficiently as a ground plane for low profile wire antennas.

The EBG parameters, namely, patch width, gap width, substrate permittivity, and substrate thickness, are evaluated respectively, and some design guidelines have been developed for an EBG surface. Two EBG surfaces with novel electromagnetic features are also proposed: the polarization dependent reflection phase is realized using rectangular patch units, and the compact unit size is achieved by cutting slots on the EBG patches.

Acknowledgment

The authors would like to thank the reviewers for their careful and in-depth evaluation of the manuscript.

References

[1] J. D. Joannopoulos, R. D. Meade, and J. N. Winn, *Photonic Crystals*. Princeton, NJ: Princeton Univ. Press, 1995.

[2] *IEEE Trans. Microwave Theory Tech. (Special Issue)*, vol. 47, Nov. 1999.

[3] Y. Rahmat-Samii and H. Mosallaei, "Electromagnetic band-gap structures: Classification, characterization and applications," in *Proc. Inst. Elect. Eng.-ICAP Symp.*, Apr. 2001, pp. 560–564.

[4] V. G. Veselago, "The electrodynamics of substances with simultaneous negative values of ϵ and μ," *Sov. Phys. Usp.*, vol. 10, no. 4, pp. 509–514, 1966.

[5] J. B. Pendry, "Negative refraction makes a perfect lens," *Phys. Rev. Lett.*, vol. 85, no. 18, pp. 3966–3969, Oct. 2000.

[6] R. A. Shelby, D. R. Smith, and S. Schultz, "Experimental verification of a negative refractive index of refraction," *Science*, vol. 292, pp. 77–79, Apr. 2002.

[7] R. W. Ziolkowski and E. Heyman, "Wave propagation in media having negative permittivity and permeability," *Phys. Rev. E, Stat. Phys. Plasmas Fluids Relat. Interdiscip. Top.*, vol. 64, no. 5, p. 056 625, Oct. 2001.

[8] N. Engheta, "An idea for thin subwavelength cavity resonators using metamaterials with negative permittivity and permeability," *IEEE Antennas Wireless Propagat. Lett.*, vol. 1, pp. 10–13, 2002.

[9] F.-R. Yang, K.-P. Ma, Y. Qian, and T. Itoh, "A uniplanar compact photonic-bandgap (UC-PBG) structure and its applications for microwave circuit," *IEEE Trans. Microwave Theory Tech.*, vol. 47, pp. 1509–1514, Aug. 1999.

[10] D. Sievenpiper, L. Zhang, R. F. J. Broas, N. G. Alexopolus, and E. Yablonovitch, "High-impedance electromagnetic surfaces with a forbidden frequency band," *IEEE Trans. Microwave Theory Tech.*, vol. 47, pp. 2059–2074, Nov. 1999.

[11] A. S. Barlevy and Y. Rahmat-Samii, "Characterization of electromagnetic band-gaps composed of multiple periodic tripods with interconnecting vias: Concept, analysis, and design," *IEEE Trans. Antennas Propagat.*, vol. 49, pp. 242–353, Mar. 2001.

[12] R. Coccioli, F. R. Yang, K. P. Ma, and T. Itoh, "Aperture-coupled patch antenna on UC-PBG substrate," *IEEE Trans. Microwave Theory Tech.*, vol. 47, pp. 2123–2130, Nov. 1999.

[13] R. Gonzalo, P. Maaget, and M. Sorolla, "Enhanced patch-antenna performance by suppressing surface waves using photonic-bangdap substrates," *IEEE Trans. Microwave Theory Tech.*, vol. 47, pp. 2131–2138, Nov. 1999.

[14] J. S. Colburn and Y. Rahmat-Samii, "Patch antennas on externally perforated high dielectric constant substrates," *IEEE Trans. Antennas Propagat.*, vol. 47, pp. 1785–1794, Dec. 1999.

[15] F. Yang and Y. Rahmat-Samii, "Microstrip antennas integrated with electromagnetic band-gap (EBG) structures: A low mutual coupling design for array applications," *IEEE Trans. Antennas Propagat.*, vol. 51, pp. 2939–2949, Oct. 2003.

[16] T. H. Liu, W. X. Zhang, M. Zhang, and K. F. Tsang, "Low profile spiral antenna with PBG substrate," *Electron. Lett.*, vol. 36, no. 9, pp. 779–780, Apr. 2000.

[17] F. Yang and Y. Rahmat-Samii, "A low profile circularly polarized curl antenna over electromagnetic band-gap (EBG) surface," *Microwave Opt. Technol. Lett.*, vol. 31, no. 3, pp. 165–168, 2001.

[18] P.-S. Kildal, "Definition of artificially soft and hard surfaces for electromagnetic waves," *Electron. Lett.*, vol. 24, pp. 168–170, Feb. 1988.

[19] ——, "Artificially soft and hard surfaces in electromagnetics," *IEEE Trans. Antennas Propagat.*, vol. 38, pp. 1537–1544, Oct. 1990.

[20] H. Mosallaei and Y. Rahmat-Samii, "Broadband characterization of complex periodic EBG structures: An FDTD/prony technique based on the split-field approach," *Electromagn.*, vol. 23, no. 2, pp. 135–151, Feb. 2003.

[21] F. R. Yang, K. P. Ma, Y. Qian, and T. Itoh, "A novel TEM waveguide using uniplanar compact photonic-bandgap (UC-PBG) structure," *IEEE Trans. Microwave Theory Tech.*, vol. 47, pp. 2092–2098, Nov. 1999.

[22] M. Rahman and M. A. Stuchly, "Transmission line-periodic circuit representation of planar microwave photonic bandgap structures," *Microwave Opt. Technol. Lett.*, vol. 30, no. 1, pp. 15–19, 2001.

[23] X. X. Zhang and F. Yang, "The study of slit cut on the microstrip antenna and its applications," *Microwave Opt. Technol. Lett.*, vol. 18, no. 4, pp. 297–300, 1998.

Fan Yang (S'96–M'03) received the B.S. and M.S. degrees from Tsinghua University, Beijing, China, and the Ph.D. degree from University of California, Los Angles (UCLA), all in electric engineering, in 1997, 1999, and 2002, respectively.

From 1994 to 1999, he was a Research Assistant with the State Key Laboratory of Microwave and Digital Communications, Tsinghua University, China. From 1999 to 2002, he was a Graduate Student Researcher in the Antenna Research, Applications, and Measurement Laboratory (ARAM), University of California, Los Angeles. Since September 2002, he has been a Research Engineer in the UCLA Antenna Laboratory. His research interests include microstrip antenna and reconfigurable antenna designs, electromagnetic band-gap structures, numerical methods in electromagnetics, and antenna measurement techniques.

Dr. Yang is Secretary of the IEEE AP Society, Los Angeles chapter.

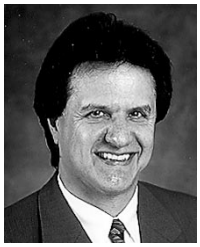

Yahya Rahmat-Samii (S'73–M'75–SM'79–F'85) received the M.S. and Ph.D. degrees in electrical engineering from the University of Illinois, Urbana-Champaign.

He is a Professor and the Chairman of the Electrical Engineering Department, University of California, Los Angeles (UCLA). He was a Senior Research Scientist at NASA's Jet Propulsion Laboratory/California Institute of Technology, Pasadena, before joining UCLA in 1989. He was a Guest Professor with the Technical University of Denmark (TUD) during the summer of 1986. He has also been a consultant to many aerospace companies. He has been Editor and Guest Editor of many technical journals and book publication entities. He has Authored and Coauthored more than 500 technical journal articles and conference papers and has written 17 book chapters. He is the Coauthor of two books entitled, *Electromagnetic Optimization by Genetic Algorithms, and Impedance Boundary Conditions in Electromagnetics* published in 1999 and 1995, respectively. He is also the holder of several patents. He has had pioneering research contributions in diverse areas of electromagnetics, antennas, measurement and diagnostics techniques, numerical and asymptotic methods, satellite and personal communications, human/antenna interactions, frequency selective surfaces, electromagnetic band-gap structures and the applications of the genetic algorithms, etc., (visit http://www.antlab.ee.ucla.edu). On several occasions, his work has made the cover of many magazines and has been featured on several TV newscasts.

Dr. Rahmat-Samii was the elected 1995 President and 1994 Vice-President of the IEEE Antennas and Propagation Society. He was appointed an IEEE Antennas and Propagation Society Distinguished Lecturer and presented lectures internationally. He was elected as a Fellow of the Institute of Advances in Engineering (IAE) in 1986. He was also a member of the Strategic Planning and Review Committee (SPARC) of the IEEE. He was the IEEE AP-S Los Angeles Chapter Chairman (1987–1989) and his chapter won the Best Chapter Awards in two consecutive years. He has been the plenary and millennium session speaker at many national and international symposia. He was one of the directors and Vice President of the Antennas Measurement Techniques Association (AMTA) for three years. He has also served as Chairman and Co-Chairman of several national and international symposia. He was also a member of UCLA's Graduate council for a period of three years. For his contributions, he has received numerous NASA and JPL Certificates of Recognition. In 1984, he received the coveted Henry Booker Award of the International Scientific Radio Union (URSI) which is given triennially to the Most Outstanding Young Radio Scientist in North America. Since 1987, he has been designated every three years as one of the Academy of Science's Research Council Representatives to the URSI General Assemblies held in various parts of the world. In 1992 and 1995, he was the recipient of the Best Application Paper Prize Award (Wheeler Award) for papers published in the 1991 and 1993 IEEE ANTENNAS AND PROPAGATION. In 1993, 1994, and 1995, three of his Ph.D. students were named the Most Outstanding Ph.D. Students at UCLA's School of Engineering and Applied Science. Seven others received various Student Paper Awards at the 1993–2002 IEEE AP-S/URSI Symposiums. He is a Member of Commissions A, B, J, and K of USNC/URSI, AMTA, Sigma Xi, Eta Kappa Nu, and the Electromagnetics Academy. He is listed in *Who's Who in America*, *Who's Who in Frontiers of Science and Technology*, and *Who's Who in Engineering*. In 1999, he was the recipient of the University of Illinois ECE Distinguished Alumni Award. In 2000, he was the recipient of IEEE Third Millennium Medal and AMTA Distinguished Achievement Award. In 2001, he was the recipient of the Honorary Doctorate in physics from the University of Santiago de Compostela, Spain. In 2001, he was elected as the Foreign Member of the Royal Academy of Belgium for Science and the Arts. He is the designer of the IEEE Antennas and Propagation Society logo that is displayed on all IEEE ANTENNAS AND PROPAGATION publications.